Received: 27 June 2022 | Revised: 9 January 2023 | Accepted: 10 January 2023

DOI: 10.1002/hyp.14810

RESEARCH ARTICLE

WILEY

Impact of land cover changes on Long-Term Regional-Scale groundwater recharge simulation in cold and humid climates

Emmanuel Dubois[1,2] | Marie Larocque[1,3] | Philip Brunner[4]

[1]Université du Québec à Montréal (UQAM), Department of Earth and atmosphere sciences and GEOTOP Research Center, Montréal, Canada

[2]Platform of Hydraulic Constructions (PL-LCH), Civil Engineering Department, Ecole Polytechnique Fédéralede Lausanne (EPFL), Lausanne, Switzerland

[3]GRIL Research Center, Département de sciences biologiques, Université de Montréal, Montréal, Canada

[4]The Center for Hydrogeology and Geothermics (CHYN), University of Neuchâtel, Neuchâtel, Switzerland

Correspondence
Emmanuel Dubois, Université du Québec à Montréal (UQAM), Department of Earth and atmosphere sciences and GEOTOP Research center, Montréal, Canada.
Email: dubois.emmanuel@courrier.uqam.ca

Funding information
Québec Ministère de l'Environnement et de la lutte contre les changements climatiques

Abstract

In cold and humid climates, warming temperatures will result in longer growing seasons, leading to land cover changes that could have long-term impacts on groundwater recharge (GWR), in addition to the direct impacts of climate change. The objective of this study was therefore to investigate whether land cover (LC) changes need to be considered when simulating long-term regional-scale potential GWR in cold and humid climates by (1) quantifying how LC changes impact simulated GWR and (2) quantifying the combined impacts of LC and climate changes on the future GWR changes. Using the region of southern Quebec (Canada) as a case study and a water budget model, this work proposes an innovative coupling of land cover change scenarios and specific future climate conditions to simulate spatially distributed transient GWR over the 1951–2100 period. The results showed that including LC changes in long-term GWR simulations produced statistically significant increases in GWR compared to using a constant LC through time (average of +13 mm). Massive afforestation taking place on agricultural lands simulated for one of the scenario chains (RCP4.5) increased GWR by reducing runoff during the snow-dominated period (average − 17 mm). The results also showed that GWR was more sensitive to climate change for scenarios that included intense land cover changes. Additionally, the spatial distribution of the LC changes influenced their simulated impacts on GWR. Considering that the methodology was computationally feasible and entirely transferrable to the new CMIP6 ensemble, LC changes should be considered systematically in long-term groundwater resources simulations.

KEYWORDS
climate change, cold and humid climates, groundwater recharge, HydroBudget Model, land cover change, regional-scale

1 | INTRODUCTION

Considering the central role of groundwater recharge (GWR) in sustainable groundwater management (Brunner et al., 2004; Foster & Ait-Kadi, 2012; Wada et al., 2010), numerous long-term simulations of GWR spanning several decades have been undertaken to anticipate possible future conditions, as reviewed for example in Atawneh et al. (2021), Larocque et al. (2019), and Smerdon (2017). In cold climate regions, warming temperatures have the potential to dramatically impact both the land cover (LC) and the hydrology (Arctic Climate Impact Assessment, 2004; Aygün et al., 2020; Pi et al., 2021). In cold regions, the main recharge period is currently during the spring thaw.

The scientific literature for such regions shows that, under warmer conditions, the main recharge period will progressively transform into a combination of a prolonged and larger fall recharge, more frequent winter recharge events due to multi-day rain periods, and less marked spring recharge due to limited snow cover (Berghuijs et al., 2014; Dubois et al., 2022; Larocque et al., 2019; Nygren et al., 2020). A warmer climate will also result in a longer growing season, which could eventually modify the LC (King et al., 2018) and impact hydrological dynamics (Hwang et al., 2018). Under these changing conditions, it is thus necessary to include LC changes when simulating future GWR over the long term (Kløve et al., 2014; Taylor et al., 2013).

Studies accounting for land use (i.e., anthropogenic land usage) and LC (i.e., the nature of the cover found on the land) in GWR simulation have led to markedly different results, depending on the study scale and the climatic and geomorphological conditions considered. Some studies have demonstrated that changes in GWR were linked to land use and LC changes at the field scale (Greenwood & Buttle, 2018; Zhang et al., 2018, 2021), at the local scale (tens of km^2; Cochand et al., 2021), or at the regional scale (thousands of km^2; Anurag et al., 2021). Others have found that land use and LC had little impact on GWR simulation, or that land use and LC impacts were smaller than those of climate change (Guerrero-Morales et al., 2020; Mohan et al., 2018; Morgan et al., 2021; Shuler et al., 2021). These differences are most likely due to the fact that it can be challenging to distinguish the impacts of climate change from the impacts of land use and LC changes on GWR, and on all components of the water budget more generally (Assani et al., 2021; Goodbrand et al., 2022; Young et al., 2019). The study scale could also determine the importance of the impacts of land use and LC changes on GWR simulations, as local impacts of changes are not necessarily visible at larger scales (Shuler et al., 2021; Zomlot et al., 2017). However, in North America, the sensitivity of water budget components to land use and LC changes seems to decrease with increased water availability, mostly from south to north and from summer to winter (Anurag et al., 2021; Healey & Rover, 2022). Agriculture favours topographic depression-focussed GWR rather than the spatially distributed recharge occurring in forests due to more intense soil frost producing more snowmelt runoff that accumulates in and infiltrates from the topographic depressions (Greenwood & Buttle, 2018). Agricultural watersheds have also been shown to have lower river baseflow than forested watersheds, because runoff usually dominates in agricultural lands, thus decreasing GWR and soil water storage (Assani et al., 2021). Although local scale GWR varies with LC, it is still unclear how LC changes will impact large scale GWR in cold and humid climates within a climate change context.

Although the recent studies on the combined impacts of LC and climate change on GWR and other water budget components have all used the recommended multi-climate scenario approach (i.e., different RCPs and climate models), the development of land use and LC scenarios greatly varied. These have ranged from participatory scenarios developed with stakeholders (Cochand et al., 2021; Shuler et al., 2021), to probabilistic LC models (Adhikari et al., 2020; Ghimire et al., 2021), or possible future changes based on past changes (Quilbé et al., 2008). These scenarios are generally devised to reflect a probable trajectory caused by expected changes in the future climate. However, GWR simulations are often performed with all possible cross-combinations and given land use and LC scenarios are not associated with specific future climate conditions. Since LC-climate feedbacks are accounted for in the climate scenarios (Taylor et al., 2012; van Vuuren et al., 2011), not associating land use and LC with specific future climatic conditions limits the possible interpretations of future GWR by mixing the signals, possibly leading to increased uncertainty (Verburg et al., 2011). Rather, Hurtt et al. (2011) standardized the ensemble of land-use scenarios that were produced by the integrated assessment models when simulating the four RCPs used in the CMIP5 project, proposing the land-use harmonization dataset. The four scenarios, corresponding to RPC2.6 to RCP8.5, were built by merging the reconstructed land-use evolution for past conditions (1500–2005 period) used in the integrated assessment models with the simulated future land-use conditions (2006–2100 period). Provided to support studies on the impacts of land use changes on Earth systems, the scenarios from Hurtt et al. (2011) have not previously been used for long-term groundwater resource simulations. Therefore, knowledge about the added impacts of LC changes on GWR within a climate change context was missing.

The objective of this study was to investigate whether LC changes need to be considered when simulating long-term regional-scale GWR in cold and humid climates. The specific objectives are (1) to quantify how LC change impacts simulated GWR and (2) to quantify the combined impacts of LC and climate changes on the future GWR changes. Spatially distributed transient GWR was simulated using the regionally calibrated HydroBudget model (HB; Dubois et al., 2021a, 2021b) over eight river watersheds located in southern Quebec (cold and humid climate, 35 800 km^2) as a regional case study. Moreover, the GWR dynamics and the expected impacts of climate change over that region are well documented with extensive past and the future GWR datasets, thus offering a potential for comparisons of scenarios simualated with LC change (Dubois et al., 2022, 2021a). In this study, GWR was simulated with observed LC changes for the 1990–2010 period and with the land-use scenarios from Hurtt et al. (2011), and a selection of 12 low-emission (RCP4.5) and high-emission (RCP8.5) climate scenarios for the 1951–2100 period.

2 | DATA AND METHODS

2.1 | Study area

The study area is located in the province of Quebec (humid continental climate), between the St. Lawrence River and the Canada–USA border, and between the Quebec–Ontario border and Quebec City (35 800 km^2) (Figure 1). It corresponds to the traditional territories of the Ho-de-no-sau-nee-ga (Haudenosaunee), Kanien'kehá:ka (Mohawk), N'dakina (Abenaki), Nanrantsouak, Penobscot, Wabanaki, Wendake-Nionwentsïo, and Wolastoqiyik (Maliseet). It includes the

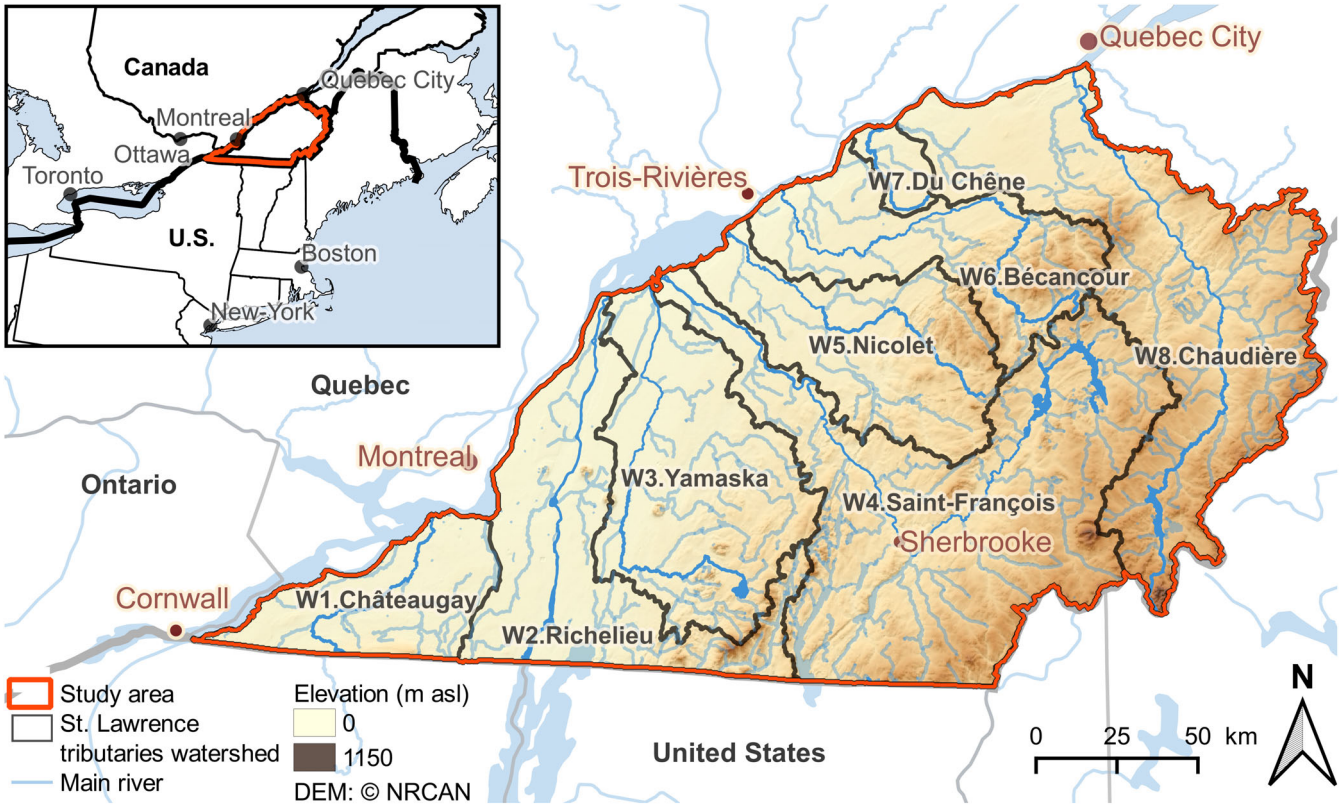

FIGURE 1 Location of the study area.

watersheds of eight tributaries of the St. Lawrence River (numbered W1 to W8 from west to east). Watersheds W1, W2, and W4 have 42%, 83%, and 15% of their total areas located in the United States, respectively. The topography is flat with elevation close to sea level near the St. Lawrence River, the Lowlands, and hilly with higher elevations in the Appalachian Mountains. The annual average temperature varies between 6.5°C (W1, west) and 3.9°C (W8, east), with a west–east cooling gradient also notable during the winter months (December to March, monthly temperature <0°C). Annual precipitation ranges between 952 mm/yr (W1) and 1123 mm/yr (W4) (Dubois et al., 2021a).

Superficial material is mainly fine (silts) and coarse (sand and gravels) materials in the uphill areas (thickness <5 m), mixed-grain size deposited in the valleys (5 m < thickness < 20 m), and clay covering sandy materials close to the St. Lawrence River (thickness > 20 m). These unconsolidated sediments from the last glaciation-deglaciation cycle unevenly cover the bedrock. Regional fractured bedrock aquifers flow from the Appalachians to the St. Lawrence River, from the south-southeast to the north-northwest. They are moderately productive and are in unconfined conditions upstream, with relatively shallow groundwater levels (2–5 m), and semi-confined to confined conditions in the valleys and in the St. Lawrence Lowlands (Rivera, 2014).

Dubois et al. (2021a) estimated the average regional potential GWR to be 12% of precipitation (139 mm/yr), while evapotranspiration represented 47% of precipitation (501 mm/yr), over the 1961–2017 period. They identified preferential recharge zones in the Appalachians, in forested areas, and over coarse deposits and outcropping bedrock. Potential GWR increased from west to east as warmer temperatures in the western watersheds (W1 to W3) were responsible for higher winter GWR rates due to more vertical inflow (the sum of rainfall and snowmelt) and lower summer and fall GWR rates (more actual evapotranspiration). The peak of the spring GWR in April, linked to snowmelt, dominated GWR in all the watersheds and corresponded to 44% of the annual GWR rates. Using 12 climate scenarios spanning 1951–2100, Dubois et al. (2022) produced scenarios of potential GWR. A significant decrease in potential GWR (change < −15 mm) was obtained for changes in annual precipitation <150 mm or cold month precipitation < +25 mm and by warming temperature by +3°C to +5°C. In contrast, a significant increase (change > +15 mm) was obtained for changes in annual precipitation >150 mm or cold month precipitation > +25 mm and increase in temperature > +2°C.

2.2 | Using the HydroBudget Model to simulate groundwater recharge

The HydroBudget model (HB) is a water budget GWR model that uses spatially distributed daily temperature, daily total precipitation, and runoff curve number (a combination of pedology, land cover, and topography) to compute gridded potential GWR (Dubois et al., 2021a, 2021b). Although using daily input data, the results are aggregated at a monthly time step with a 500 m × 500 m spatial resolution. It was

developed for long-term and regional-scale simulations in cold and humid climates, assuming that surface watersheds match hydrogeological watersheds and those rivers drain unconfined aquifers. It is driven by eight parameters that need to be calibrated (Table 1). For each daily time-step, HB computes the snow accumulation and melt (parameters 1 and 2), tests whether the soil is frozen (parameters 3 and 4), and partitions the superficial runoff (based on the runoff curve number method) (parameters 5 and 6) from the water that infiltrates into a conceptual soil reservoir (parameter 7). The actual evapotranspiration corresponds to the minimum between the potential evapotranspiration calculated using the formula of Oudin et al. (2005) and the available water in the soil reservoir. Part of the residual soil reservoir water is mobilized as potential GWR (parameter 8). Details of HB calculations can be found in Dubois et al. (2021a, 2021b). Since HB does not simulate percolation out of the unsaturated zone, the potential GWR represents a maximum GWR that could reach the saturated zone. For simplification, the simulated potential GWR will be herein referred to as GWR.

Over the same study area, Dubois et al. (2021a) calibrated HB using a multi-objective automatic calibration with measured river flow from 51 gauging stations over the 1961–2017 period and baseflow estimates (regressive filter on river flow time series). The simulated variables had a low uncertainty (≤ 10 mm/yr). The calibrated model was also used by Dubois et al. (2022) to produce 12 GWR scenarios over the 1951–2100 period. These simulations were undertaken with the hypothesis that the LC was steady over time.

2.3 | Climate datasets

2.3.1 | Past climate (1990–2010)

Similarly to Dubois et al. (2021a), the spatially interpolated daily temperature and precipitation data (10 km × 10 km spatial resolution) from Bergeron (2016) were used. They were produced based on data from 251 meteorological stations, and the root mean square error over the 1961–2017 period was 3 mm/d for daily precipitation, 2.5°C for minimum daily temperature, and 1.5°C for maximum daily temperature.

2.3.2 | Climate scenarios

A subset of 12 climate scenarios was derived from an ensemble of 54 climate simulations provided by 29 global climate models from the Coupled Model Intercomparison Project—Phase 5 (CMIP5) driven by RCP4.5 and RCP8.5 future greenhouse gas concentrations (Figure 2). Presented by Dubois et al. (2022), the 12-member ensemble (Table 2) was created using the k-means clustering method proposed by Casajus et al. (2016) in order to maximize the variability represented in the future conditions. The selection was based on ten criteria of changes in annual and seasonal temperature and precipitation conditions between the 1951–2010 and the 2041–2070 periods (not considering the RCPs). The 12 selected simulations were bias-corrected to a 1981–2010 reference dataset (Natural Resources Canada gridded observation database) (Hopkinson et al., 2011; Hutchinson et al., 2009) and downscaled to the reference 10 km × 10 km resolution using the quantile mapping approach of Mpelasoka and Chiew (2009).

2.4 | Land cover data sets

2.4.1 | Land cover classes

Land cover of the study area was classified into five classes, that is, agriculture, forest, wetlands, water, and urban. Agriculture referred to areas with grassland, vegetation (tree and crops), bare soil, and small water bodies found in agricultural areas. Forest referred to the areas covered by trees that could also be used for wood harvesting.

TABLE 1 Description of the HydroBudget parameters and regionally calibrated values.

Parameter			Regionally calibrated values from Dubois et al. (2021a)
Snowmelt model	1.	Air temperature threshold for snowmelt (°C)	1.4
	2.	Melting rate of the snowpack (mm.°C^{-1}.d^{-1})	4.9
Freezing soil conditions	3.	Air temperature threshold for soil frost (°C)	−15.9
	4.	Duration of air temperature threshold to freeze the soil (d)	16.4
Runoff	5.	Time constant to consider the soil in dry or wet conditions based on previous precipitation event (d)	3.9
	6.	Partitioning between runoff computed with the RCN method and infiltration into the soil reservoir (–)	0.6
Lumped soil reservoir	7.	Soil reservoir storage capacity, maximum height of water stored in a 1 m soil profile (mm)	385
	8.	Fraction of soil water that produces deep percolation at each daily time step (–)	0.06

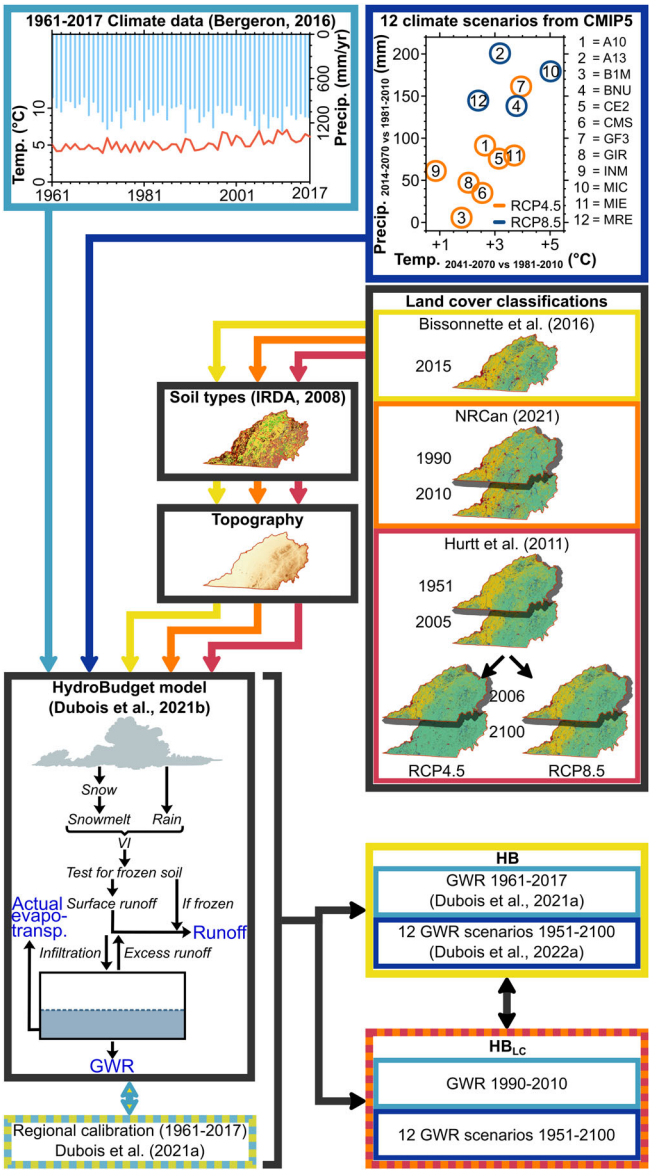

FIGURE 2 Conceptual workflow for the simulation of long-term groundwater recharge (GWR) with the HydroBudget model with constant (HB) and varying (HB_{LC}) land cover (LC) over past meteorological conditions (1961–2017) and future climate conditions (1951–2100). For detailed LC maps, refer to supp. Figure A1.

Wetlands referred to the areas of hydrophilic vegetation temporarily or permanently flooded. Water LC referred to surficial water bodies. Urban LC referred to areas with impervious surfaces, low density of trees, vegetation (gardens and parks), as well as bare soil locally found in the anthropogenic and urban environments.

2.4.2 | Constant land cover

The GWR simulations from Dubois et al. (2021a, 2022)) were based on the LC map of Bissonnette et al. (2016), developed for the Quebec Ministry of Environment. The LC classification was done at a 30 m × 30 m spatial resolution based on provincial and national censuses spanning 2010–2016 (average year 2015). The LC map was resampled at a 500 m × 500 m spatial resolution using a majority rule and reclassified into the five LC classes.

TABLE 2 Selected climate scenarios.

Model source	Code	RCP
Commonwealth Scientific and Industrial Research Organization (CSIRO), Australia and Bureau of Meteorology (BOM), Australia (ACCESS1-0_rcp45_r1i1p1)	A10	4.5
Commonwealth Scientific and Industrial Research Organization (CSIRO), Australia and Bureau of Meteorology (BOM), Australia (ACCESS1-3_rcp85_r1i1p1)	A13	8.5
Beijing Climate Center, China Meteorological Administration, China (bcc-csm1-1-m_rcp45_r1i1p1)	B1M	4.5
College of Global Change and Earth System Science, Beijing Normal University (BNU), China (BNU-ESM_rcp85_r1i1p1)	BNU	8.5
Canadian Center for Climate Modelling and Analysis (CCCma), Canada (CanESM2_rcp45_r1i1p1)	CE2	4.5
Centro Euro-Mediterraneo sui Cambiamenti Climatici Climate Model, Italy (CMCC-CMS_rcp45_r1i1p1)	CMS	4.5
Geophysical Fluid Dynamics Laboratory (GFDL), USA (GFDL-CM3_rcp45_r1i1p1)	GF3	4.5
National Aeronautics and Space Administration (NASA)/Goddard Institute for Space Studies (GISS), USA (GISS-E2-R_rcp45_r6i1p3)	GIR	4.5
Institute for Numerical Mathematics (INM), Russia (inmcm4_rcp45_r1i1p1)	INM	4.5
Japan Agency for Marine-Earth Science and Technology, Atmosphere and Ocean Research Institute (The University of Tokyo), National Institute for Environmental Studies, Japan (MIROC-ESM _rcp45_r1i1p1)	MIC	8.5
Japan Agency for Marine-Earth Science and Technology, Atmosphere and Ocean Research Institute (The University of Tokyo), National Institute for Environmental Studies, Japan (MIROC-ESM-CHEM_rcp85_r1i1p1)	MIE	4.5
Meteorological Research Institute, Japan (MRI-ESM1_rcp85_r1i1p1)	MRE	8.5

2.4.3 | Observed land cover change (1990–2010)

Agriculture and Agri-Food Canada provided Canada-wide LC maps with 15 classes for 1990, 2000, and 2010 with a 30 m × 30 m spatial resolution (NRCan, 2021). The LC classification was performed based on national censuses and the ground-truthing showed an overall

accuracy of 84%, 87%, and 93%, for the 3 years, respectively. To meet the needs of the current study, these maps were resampled with a 500 m × 500 m spatial resolution using a majority rule and reclassified into the five LC classes. To obtain LC data at a yearly time step, the changes in LC between the three reclassified and resampled maps were randomly assigned to a year between each map.

2.4.4 | Land cover change scenarios (1951–2100)

The global land-use harmonization dataset harmonized a historical reconstruction of land use (1500–2005 period; Klein Goldewijk et al., 2010) with the four simulations of future land use (2006–2100 period) produced by the integrated assessment models along the RCPs (Chini et al., 2014; Hurtt et al., 2011). The land use associated with RCP4.5 and RCP8.5 were simulated by the Global Change Assessment Model (GCAM; Thomson et al., 2011) and Model for Energy Supply Strategy Alternatives and their General Environmental Impact (MESSAGE; Riahi et al., 2011) integrated assessment models respectively. While the driving forces for LC change in RCP4.5 scenario were associated with climate policies valuing carbon in natural vegetation, LC change in RCP8.5 scenario was mainly driven by high population growth and low technology development rate (van Vuuren et al., 2011).

The land-use harmonization scenarios considered land-use changes through time with an annual time step on 0.5° × 0.5° cells, and included the proportion of specific land-use classes on each cell, that is, cropland, pasture, primary land (untouched primary vegetation), secondary land (natural land recovering from anthropogenic activities), and urban land. The conversion from land use to LC was done considering both cropland and pasture as agricultural lands and, following the dataset classification rules, the sum of primary and secondary lands as forest. Superficial water bodies were considered constant in the database. The four LC classes (agriculture, forest, water, and urban) were used to downscale the scenarios to a 500 m x 500 m spatial resolution over the study area. The 1990 proportional LC from Hurtt et al. (2011) was distributed onto the overlapping 500 m × 500 m pixels from the resampled and reclassified 1990 LC map from NRCan (2021), using when possible the LC classes from NRCan. Where needed, changes in classes were randomly assigned to the closest pixels of the targeted LC class identified with a 9 × 9 moving window, assuming that a change in LC could only occur next to a pixel of the targeted new LC class (closest neighbour analysis). Using the newly downscaled 1990 LC map, the annual LC changes from the land-use harmonization dataset were then assigned forward from 1991 to 2100 and backward from 1989 to 1951.

Wetlands were not specifically considered in the conversion of the land-use harmonization dataset to LC maps and were most likely confused with forest in the primary and secondary lands. In order to simplify the comparison between the different LC classifications, wetlands were directly imported from the LC classification of Bissonnette et al. (2016) to the downscaled LC scenarios from Hurtt et al. (2011) and considered constant through time, similarly to the superficial water bodies.

2.5 | Runoff curve numbers

The runoff curve numbers were calculated for each cell using pedology data, land cover classification, and average slope (USDA-NRCS, 2004, 2007). The method was specifically adapted for the province of Quebec by Gagné et al. (2013) and Monfet (1979) with the IRDA (2008) pedological maps. As LC is one of the parameters needed to compute the runoff curve number, time-varying LC maps can be used to compute transient values of spatially distributed runoff curve number values, assuming that slope and pedology remain constant over time.

2.6 | Groundwater recharge comparison, periods, and datasets

In the current study, the HB model was run using time-variant spatially distributed runoff curve number values derived from the LC classifications from NRCan (2021; 1990–2010 period) and from Hurtt et al. (2011; 1951–2100 period) to provide spatially distributed transient GWR accounting for LC changes (Figure 2). These simulations are hereafter referred to as HB_{LC}. To facilitate comparison with GWR simulations based on constant LC, the regionally calibrated HB parameters reported in Dubois et al. (2021a, 2022), were also used here.

In order to understand the effect of LC changes on long-term GWR simulations, the results obtained using HB_{LC} were compared to the GWR simulated with HB over the 1990–2010 period (Dubois et al., 2021a) and over the 1951–2100 period (Dubois et al., 2022) (Figure 2). The performance of HB and HB_{LC} were compared using the Kling–Gupta Efficiency (KGE) calculated (1) with monthly measured and simulated total flow (KGE_{qtot}) and (2) with the monthly baseflow (estimated using the Lyne and Hollick recursive filter) and simulated GWR (KGE_{qbase}). The comparison was done over 1990–2010 because observed river flow data were available for all the watersheds for this period. For the 1951–2100 period, the simulation period was divided into four 30-year sub-periods, that is, 1981–2010 as the reference period (also used for bias correction of the climate scenarios), and three future periods, 2011–2040, 2041–2070, and 2071–2100. Each 30-year sub-period was compared to the previous one and to the 1981–2010 reference period to observe the simulated range in future GWR and to identify future GWR changes.

The annual similarity between the transient LC datasets and the constant LC classification was used to quantify the evolution of LC over time. It represents the number of pixels with the same LC classification in two datasets for a given year (expressed in % of the considered area). The afforestation rate, representing the forest development of the study area, was also used as a second indicator of LC changes (% of forest in the considered area).

3 | RESULTS

3.1 | Land cover evolution in the study area

The resampled and reclassified LC map from Bissonnette et al. (2016) showed that the average LC in 2015 in the study area was composed of forest (49.5%), agriculture (38.0%), wetlands (5.7%), urban (4.8%), and water (2.0%) (based on data acquired during the 2010–2016 period) (Figure 3a; supp. Figure A1). The resampled and reclassified LC dataset from NRCan (2021) showed an increase in urban and agricultural lands at the expense of forested lands between 1990 and 2010, estimating more urban and forested area than the constant LC from Bissonnette et al. (2016) (Figure 3b), and resulting in an annual similarity of 72.8% in 2010 (supp. Figure A1). The downscaled LC classification from Hurtt et al. (2011) also showed an urbanization of the study area through time, with the most important changes over the 1951–2005 period (+1% of urban areas over the entire study area) (supp. Figure A1). With this dataset, future conditions include a stabilization of urban area for the RCP4.5 scenario and a very small increase for the RCP8.5 scenario (+0.3% until 2100). The downscaled scenarios from Hurtt et al. (2011) showed a 10% increase in forested area at the expense of agriculture over the 1951–2005 period. This trend continued for the RCP4.5 scenario until forested area represented 89.9% of the study area in 2100 (0.4% for agriculture). In comparison, forest cover and agricultural lands stabilized in 2006 for the RCP8.5 scenario. Overall, the LC classification downscaled from Hurtt et al. (2011) was relatively close to the LC classification from NRCan (2021) in 1990, with an annual similarity of 80.8% (Figure 3c). The constant LC classification of Bissonnette et al. (2016) had an annual similarity of 65.7% and 72.5% in 2015 for the RCP4.5- and RCP8.5-based scenarios, respectively (not shown). The LC scenarios from Hurtt et al. (2011) mainly differed from the other LC classifications in their underestimation of urban area (classified instead as forest and agriculture), the addition of the wetlands from the constant LC classification (mainly at the expense of forest), and the confusion between forest and agricultural area.

3.2 | Water budget over the 1990–2010 period

Over the study area, annual precipitation ranged between 957 mm (2001) and 1331 mm (1990), and temperature between 4.3°C (1992) and 7.0°C (2010), with no significant trends (Figure 4a). The simulation using HB_{LC} produced significantly lower runoff than that of HB (−19 mm/yr), compensated by significantly higher GWR (12 mm/yr) (Tukey test, $p < 0.05$) for the 1990–2010 period (Figure 4b, d). During this period, a slight decrease in forested area was included in HB_{LC} (59.4% in 1990 to 56.3% in 2010), remaining higher than forested area in HB (49.5%) (Figure 3). The interannual distribution of low and high annual runoff, actual evapotranspiration, and GWR rates (Figure 4b–d) were very similar for the two versions of the model. At the seasonal scale (winter, spring, summer, and fall), there were also no significant differences between the results obtained with the two datasets (results not shown), except in W7 when the HB_{LC} GWR from December to March was statistically higher than that of HB. No significant annual or seasonal trends were found in the simulated variables with either dataset. The KGEs computed over the 1990–2010 period were also similar for the two datasets (Table 3), indicating that the quality of the simulations was comparable for past conditions.

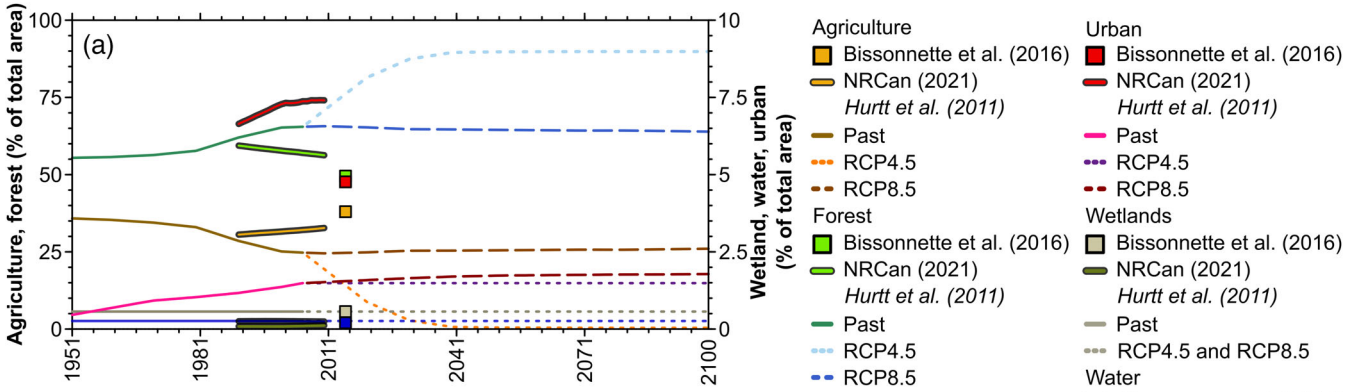

(b)

Year 2015 (Bissonnette et al., 2016) \ Year 2010 (NRCan, 2021)	agr.	for.	wet.	wat.	urb.
agr.	37394	11918	397	436	3313
for.	7018	58721	451	657	2830
wet.	422	6517	669	158	202
wat.	197	470	42	1868	273
urb.	985	1537	69	311	3801

(c)

Year 1990 (NRCan, 2021) \ Year 1990 (Hurtt et al., 2011)	agr.	for.	wet.	wat.	urb.
agr.	36219	6202	375	219	0
for.	2524	73193	6674	1155	0
wet.	40	510	572	65	0
wat.	0	1354	178	2032	0
urb.	1347	5982	169	202	1644

FIGURE 3 Land cover changes over the study area (a), comparison in number of pixels between the resampled and reclassified LC classifications between the year 2015 from Bissonnette et al. (2016) and the year 2010 from NRCan (2021) (b), and the year 1990 between NRCan (2021) and Hurtt et al. (2011) (c) (total number of pixels = 140 656). For detailed LC maps, refer to supp. Figure A1.

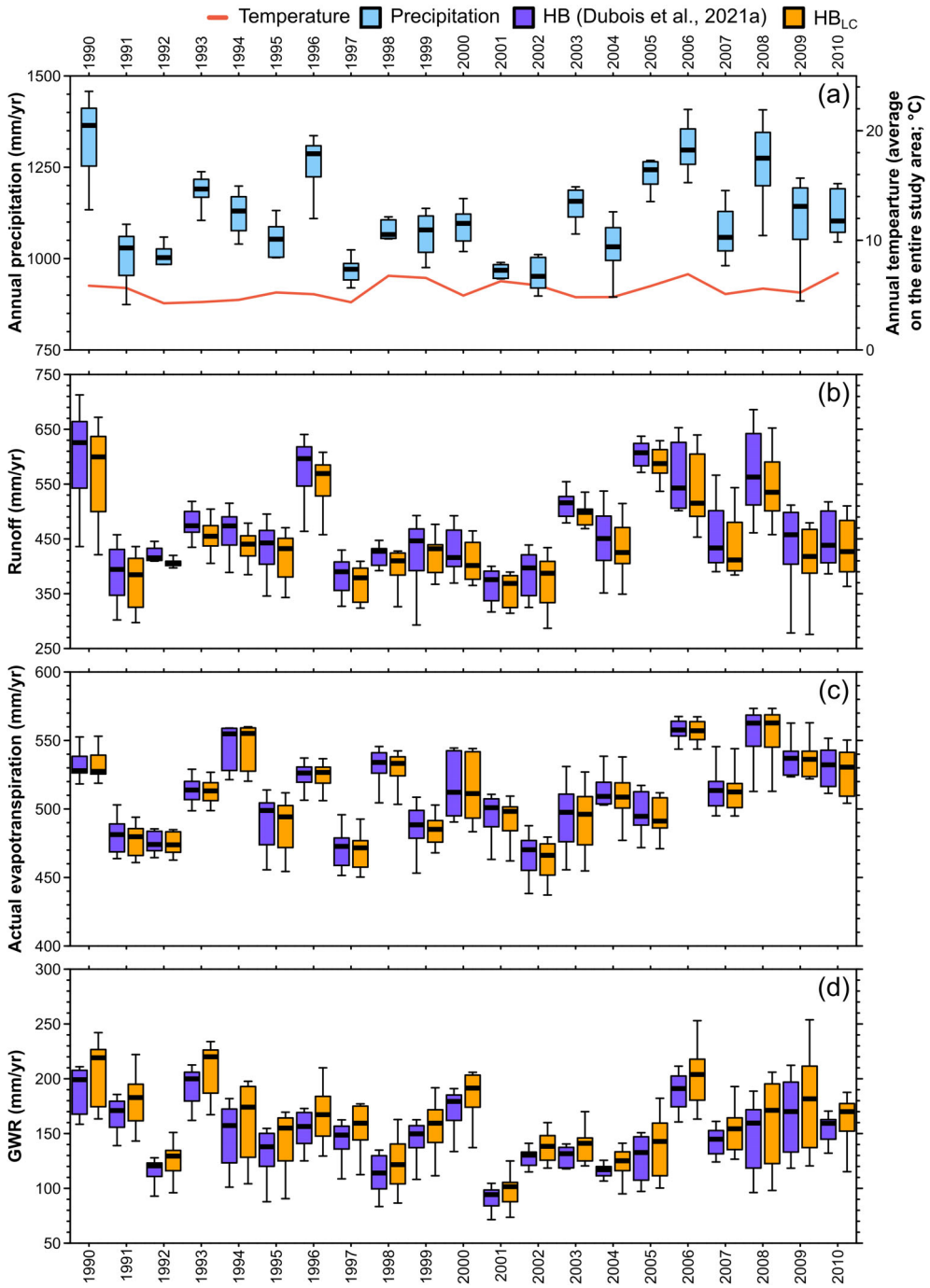

FIGURE 4 Annual precipitation and temperature (a) and simulated runoff (b), actual evapotranspiration (c), and GWR (d) using HB (Dubois et al., 2021a) and HB_{LC} for the eight watersheds over the 1990–2010 period.

3.3 | Simulation of groundwater recharge under global changes

The ensemble of HB_{LC} GWR ranged between 117 (W1, 1981–2010 period) and 205 mm/yr (W7, 2071–2100 period) (Figure 5, Supp. Figure A1). It represented an average difference of +13 mm/yr in comparison to HB (Dubois et al., 2022) over the entire study area and for the 1981–2100 period, ranging from −9 (W1, 1981–2010 period) to +27 mm/yr (W3, 2041–2070 period). The two LC datasets produced similar results, with GWR from the HB_{LC} ensemble generally higher but overlapping with the HB results of Dubois et al. (2022).

The average uncertainty in the future GWR using HB_{LC}, represented here as the standard deviation of the 12 scenarios, was 34 mm/yr, compared to 31 mm/yr for HB (Figure 5). As in Dubois et al. (2022), the uncertainty and the average GWR using HB_{LC} increased from the warmer western watersheds to the colder eastern watersheds (W1 to W8). For both ensembles, the uncertainty remained relatively constant through time in the western watersheds, from W1 to W3, and slightly decreased over time in the eastern watersheds, from W4 to W8.

Similar to the HB ensemble, the annual maximum and minimum of the HB_{LC} ensemble were simulated for RCP4.5 and RCP8.5

TABLE 3 Kling Gupta Efficiency between simulated total flow and observed river flow (KGE_{qtot}) and simulated GWR and estimated baseflow (KGE_{qbase}) over the 1990–2010 period (1993–2010 for W7) for the dataset of Dubois et al. (2021a); HB) and the simulation of GWR with HB_{LC}.

		HB		HB_{LC}	
	Nbr. Of stations	KGE_{qtot}	KGE_{qbase}	KGE_{qtot}	KGE_{qbase}
W1	2	0.77	0.62	0.76	0.61
W2	5	0.70	0.64	0.70	0.64
W3	14	0.77	0.63	0.77	0.61
W4	2	0.85	0.73	0.83	0.71
W5	3	0.82	0.73	0.82	0.73
W6	5	0.81	0.62	0.82	0.68
W7	2	0.89	0.77	0.82	0.59
W8	5	0.78	0.73	0.78	0.76

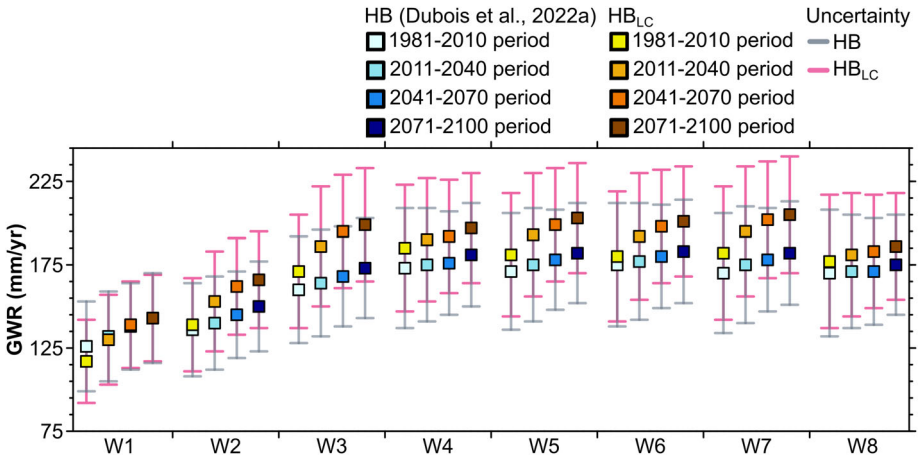

FIGURE 5 Thirty-year evolution of mean GWR and standard deviation (mm/yr) using HB (Dubois et al., 2022) and HB_{LC} scenarios for the eight watersheds (W1 to W8).

scenarios, depending on the period and the watershed (Supp. Figure A2). Both significant increase and decrease in GWR between successive 30-year periods were simulated by the two ensembles. The statistically significant changes were the same for HB_{LC} and with HB, except for the MIE climate scenario (RCP4.5) in W1 and W2 between the 2011–2040 period and the 2041–2070 period. HB_{LC} produced more significant GWR increases for the RCP4.5 scenarios than HB for all watersheds (except W4 and W8) during the 2011–2040 period and for W1 to W3 during the 2041–2070 period.

3.4 | Analysing specific conditions

3.4.1 | Agriculture and Forest

To identify the hydrological processes associated with the main LC over the study area and responsible for changes in the regional water budget, changes in GWR using HB and HB_{LC} between the future periods (2011–2014, 2041–2070, and 2071–2100) and the reference period (1981–2010) were analysed for agricultural and forested lands (Figure 6). Simulated GWR ranged between 140 (HB_{LC}, RCP4.5, 1981–2010 period) and 176 mm/yr (HB, RCP8.5, 2071–2100 period) for agricultural lands and between 192 mm/yr (HB_{LC}, RCP4.5, 1981–2010 period) and 249 mm/yr (HB, RCP8.5, 2071–2100 period) for forested lands. With an annual similarity in LC varying between 70% and 75% between the two ensembles, the simulated GWR from HB_{LC} for both agriculture (RCP4.5 scenarios) and forest was significantly lower than that of HB during the reference period (Tukey test, $p < 0.05$; sign "- "under the boxplots). Forest GWR using HB_{LC} was also significantly lower than that using HB only for RCP4.5 scenarios for the remaining three future periods. However, the difference decreased over time. In comparison to HB, the results obtained using HB_{LC} were more often statistically significant GWR increases between the future periods and the reference period (Figure 6b; blue background), up to +51 mm/yr for RCP8.5 scenarios between the 2071–2100 period and the 1981–2010 period. Runoff and actual evapotranspiration for agriculture and forest area were not significantly different between the two ensembles and both increased significantly over time (not presented here).

3.4.2 | Constant and transient land cover

Changes in GWR (ΔGWR) simulated using HB (Dubois et al., 2022) and HB_{LC} and between the three 30-year future periods and the 1981–2010 period were represented for each climate scenario and for each watershed (Figure 7a to c; temporal changes within each ensemble). Significant ΔGWR simulated using HB_{LC} were all >0

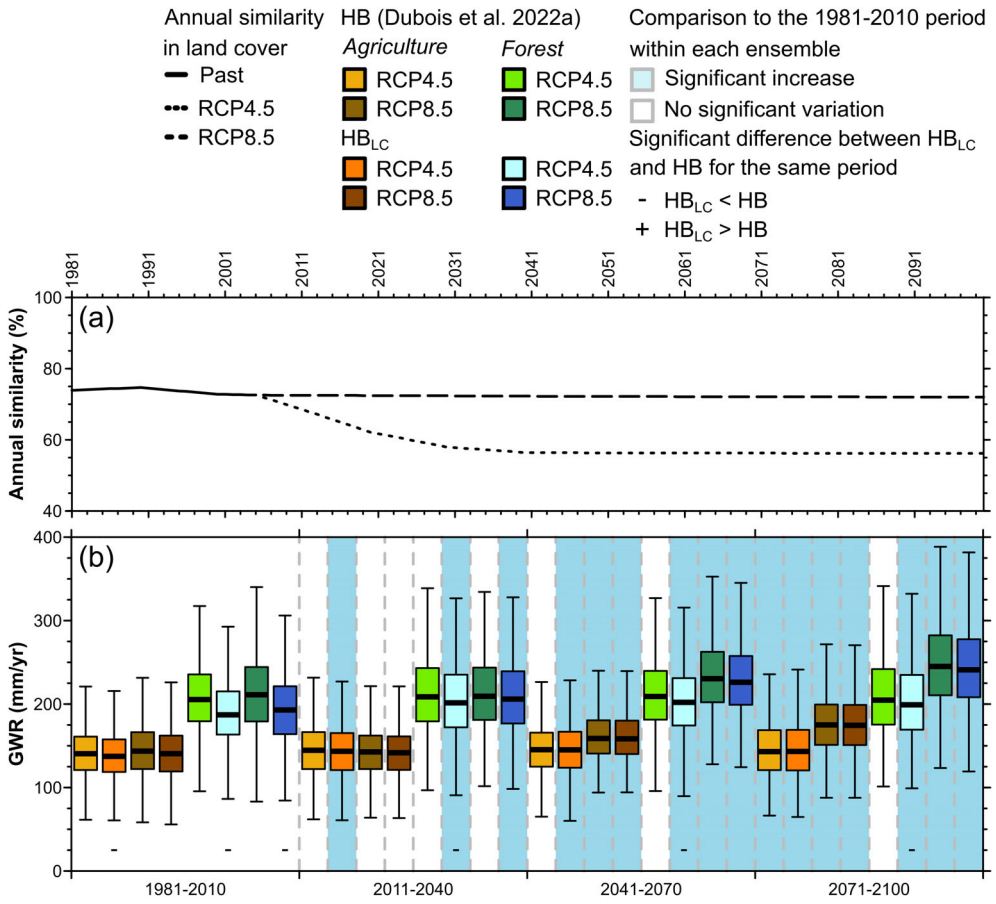

FIGURE 6 Annual similarity in land cover between the downscaled LC classifications from Hurtt et al. (2011) and Bissonnette et al. (2016) (a) and GWR over agriculture and forested lands using HB (Dubois et al., 2022) and HB_{LC} for the eight watersheds over the 1981–2100 period (b).

(i.e., increases in GWR), between +19 mm (W1, CE2, RCP4.5, 2011–2040 period) and + 69 mm (W5, MRE, RCP8.5, 2071–2100 period). RCP4.5 and RCP8.5 scenarios all produced a comparable range of significant ΔGWR. However, scenarios based on RCP4.5 produced significant ΔGWR for smaller changes in temperature (Δ*T*) and precipitation (Δ*P*) than scenarios based on RCP8.5 (Figure 7a, b). The footprint (coloured and hatched areas) of ΔGWR produced by each model version for each RCP showed the similar results for HB_{LC} and HB for simulations based on RCP8.5. However, the HB_{LC} simulations based on RCP4.5 produced significant ΔGWR for a wider range of ΔT and ΔP and no significant ΔGWR <0 (i.e., decreases in GWR), thus extensively modifying the footprint of the significant ΔGWR. ΔGWR resulting from HB_{LC} simulations based on RCP4.5 were also higher than those resulting from HB (Figure 7c). The upper limit of non-significant ΔGWR was +17 mm for HB and + 19 mm for HB_{LC}.

Differences in GWR between the two ensembles as a function of runoff difference between December and May (winter and spring seasons) for all climate scenarios and for all watersheds for the three 30-year future periods showed that GWR differences were only significant and > 20 mm with RCP4.5 scenarios for W2, W3, W5, and W7 (i.e., HB_{LC} > HB). They were all associated with an almost equal difference in runoff from December to May, < −17 mm (Figure 7d). This indicates that the GWR differences between the two ensembles were thus mostly due to a deficit in runoff simulated using HB_{LC} during the period of the year affected by snow accumulation and melting.

Non-significant GWR difference <0 mm (i.e., HB_{LC} < HB) were only simulated for RCP8.5 scenarios in W1 (all periods) (Figure 7d, supp. Figure A3). Although simulations using HB_{LC} based on RCP4.5 scenarios were significantly different from HB starting with an annual similarity in LC of 65.6% (W7), simulations based on RCP8.5 and reaching a minimum annual similarity in LC of 62.7% were not significantly different (supp. Figure A3). Significant GWR differences were only, but not consistently, obtained for a difference in forest area > 32% (W7, 2011–2040 period). Although GWR simulated using HB_{LC} was significantly higher than that of HB in W3 for all RCP4.5 climate scenarios, all periods, and with a difference in forest area of between 50.7% and 59.8%, forest area differences between 49.8% and 60.8% in W2 did not systematically produce significant differences between the two ensembles. Higher forest areas in HB_{LC} thus tended to produce significant differences more often, but not systematically.

4 | DISCUSSION

4.1 | Impact of land cover changes on regional groundwater recharge

The results show that including transient LC changes increased simulated GWR, and that this increase was within the uncertainty range of

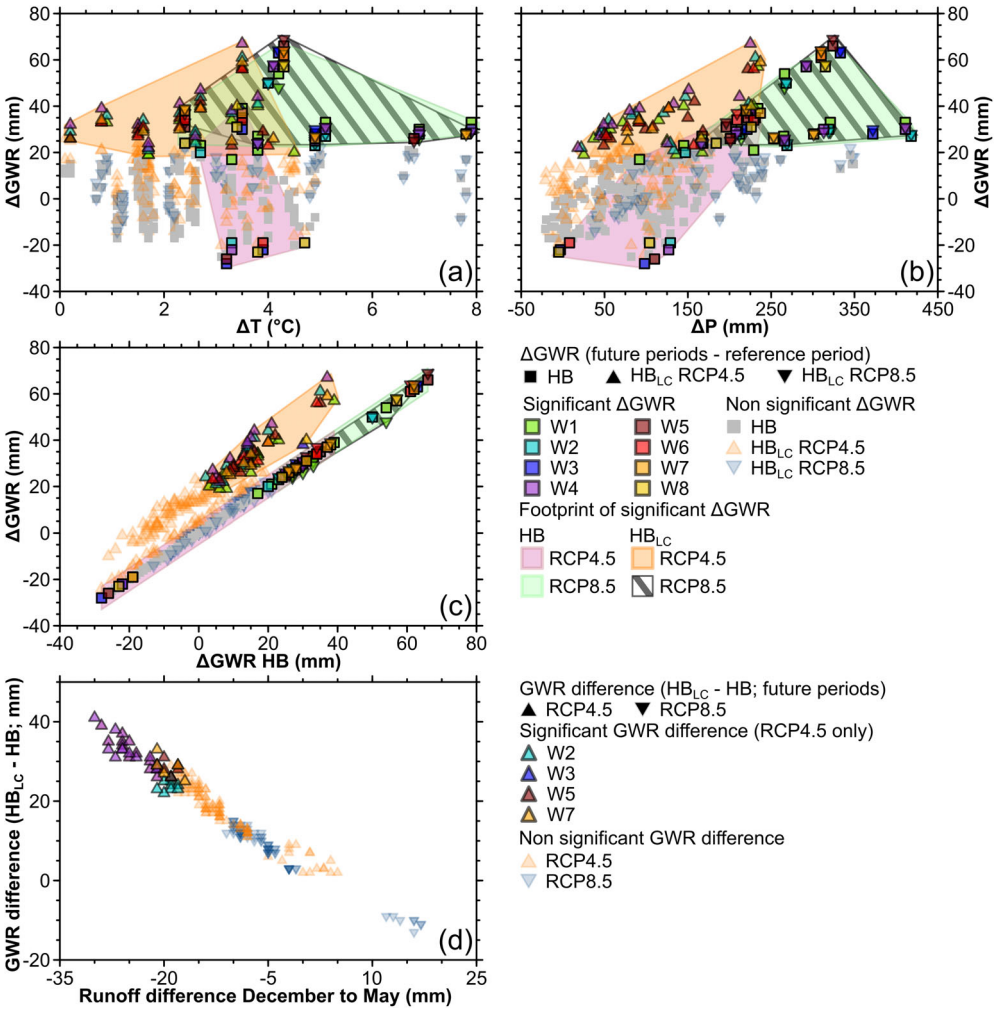

FIGURE 7 Changes in GWR (ΔGWR) using HB and HB_{LC} between the 2011–2040, 2041–2070, and 2071–2100 periods and the 1981–2010 period as a function of changes in temperature (Δ*T*) (a), as a function of changes in precipitation (Δ*P*) (b), and as a function of changes in ΔGWR using HB (c); differences between HB_{LC} and HB (Dubois et al., 2022) for the 2011–2040, 2041–2070, and 2071–2100 periods as a function of runoff difference from December to May between HB_{LC} and HB (d).

the future conditions (Figure 5). Over the 1990–2010 period, this higher GWR was mostly due to an increase in forest area that reduced the simulated runoff and boosted the amount of water infiltrating to the lumped soil reservoir (Figure 4). During the 1951–2100 period, the scenarios with high afforestation at the expanse of agriculture in RCP4.5 produced major decreases in runoff during the period that was influenced by snow storage and snowmelt (winter and spring) using HB_{LC}, causing significant increases in GWR compared with HB (Figure 7). This is consistent with the results of Dubois et al. (2021a) over the study area, who showed that GWR was limited or null during the growing season and mainly occurred when actual evapotranspiration was low and more water was available for GWR (fall to early spring).

In the similar cold climate environments, the roles of agriculture and forest in GWR changes seems to be mainly linked to the cold period. For example, Morgan et al. (2021) did not find a clear difference in depression-focussed GWR between grassland and cropland environments in the Canadian Prairies due to very similar snowmelt runoff dynamics. Destouni et al. (2013) and Jaramillo et al. (2013) linked historical agricultural development at the expense of grassland to increases in runoff and actual evapotranspiration in several watersheds in Sweden, thus reducing the available water for recharge. Meanwhile, increases in spring and fall minimum river flows in southern Quebec (Canada) were linked to a reduction in agriculture area in the 1950 s and were interpreted as an increase in GWR (Assani et al., 2021). Alternatively, Greenwood and Buttle (2018) showed that agricultural LC notably increased the depression-focussed GWR compared with forested area in a complex and highly permeable moraine deposit in southern Ontario (Canada), mainly due to more intense winter soil frost, producing more snowmelt runoff that accumulated in highly permeable topographical depression, thus favouring GWR compared with agriculture area. Overall, the scientific literature links hydrologic changes induced by LC to its influence on winter soil frost and spring thaw. One of the main contributions of this study was to show that loss in snowmelt runoff was the main hydrological process responsible for increase in regional-scale GWR when afforestation was taking place at the expanse of agricultural lands. Forests reduced snowmelt runoff, leaving more water available for recharge during the dormant season when actual evapotranspiration is very limited.

This study also shows that, despite the increase in simulated GWR, transient LC did not impact the inter-annual GWR dynamics, as HB_{LC} reproduced the annual high and low GWR and the long-term GWR changes simulated by HB for each climate scenario (Figure 4, Supp. Figure A2). The RCP4.5 scenarios, associated with the most

extreme LC changes, did not systematically produce the highest or the lowest GWR rates, and both increases and decreases in GWR were simulated with RCP4.5 and RCP8.5 when comparing successive 30-year periods (Supp. Figure A2).

4.2 | Implied processes

The increase in forest area in HB_{LC} produced a greater increase in GWR compared to HB due to higher GWR in forest area compared to agriculture area (Figure 6). Dubois et al. (2021a) showed that low GWR rates over agriculture lands were associated with local surface conditions, as agriculture was mainly located in the lowlands and in relatively flat areas covered with low-permeability surficial deposits, and receiving less precipitation. The reduced GWR rates (and increased runoff and actual evapotranspiration rates) simulated using HB_{LC} compared with HB over the 1981–2010 period were mostly due to afforestation taking place on low-permeability surficial deposits previously occupied by agriculture in the lowlands (Figure 6, Supp. Figure A4). Similarly, Assani et al. (2021) and Goodbrand et al. (2022) identified average slope and soil water storage as countering the impact of agricultural development on forested land and wood harvesting on the river flow of six watersheds of different sizes in southern Quebec (Canada) and three headwater watersheds in Alberta (Canada). While an increase in fall and spring rainfall was the second reason identified by Assani et al. (2021) for the increase in minimum flow during these seasons in southern Quebec, Goodbrand et al. (2022) found that climate variability also reduced impacts of land-use changes on river flow. Similarly, moister future conditions expected in southern Quebec counter balanced the decrease in GWR rates simulated using HB_{LC} due to afforestation taking place on low-permeability surficial deposits, thus reducing the impact of LC changes on GWR (Figure 6). Additionally, HB_{LC} only resulted in significant changes in GWR different to those resulting from HB during the peak of LC changes (i.e., the 2011–2040 period), while the changes in climatic conditions were responsible for long-term changes (Supp. Figure A2). Considering the sensitivity of GWR to local geomorphological and climate conditions, this study demonstrated that the LC-induced changes in GWR highly depended on the spatial distribution of LC changes. This observation can most likely be extended to the other hydrological processes involved in the water budget.

The addition of transient LC data in HB_{LC} produced significant increases in GWR when compared to the 1981–2010 period, while HB also produced GWR decreases with relatively small ΔP and major ΔT (Dubois et al., 2022). The changes simulated for the RCP8.5 scenarios were largely similar between the two ensembles because the LC scenario for this RCP downscaled from Hurtt et al. (2011) had only minor LC changes over time. The simulations for RCP4.5 scenarios produced significant GWR changes for a wider range of ΔP and ΔT using HB_{LC}, as they were associated with intense LC changes. While studying the impact of historical forest harvesting on river flow, Young et al. (2019) found that the more disturbed headwater catchments in the central Appalachian Mountains (USA, approximately 10 ha) were more sensitive to temperature changes. Despite the larger scale of the current study, another contribution of this work was to show that more intense LC changes increased the sensitivity of GWR to both changes in temperature and precipitation.

Another novel aspect of this work was showing that differences in GWR between the two ensembles for the three future periods were only significant when they were > 20 mm (HB_{LC} > HB) and were only simulated with annual similarity in LC < 65%, corresponding to an increase in forest area > 32% and a difference in runoff from December to May < −17 mm. However, even though intense LC changes produced significant changes in GWR in some watersheds, this was not observed in all watersheds.

The uncertainty in the future GWR simulated using HB_{LC} was only slightly higher than that of HB (+2.3 mm/yr; +7%), thus showing that the chosen methodology, with combined climate and LC scenarios associated with the two RCPs, did not markedly increase the uncertainty in simulated future conditions (Figure 5).

4.3 | Limitations and recommendations

This study showed that integrating scenarios of LC change into the simulation of future GWR led to a clearer signal in GWR changes, with a small increase in the uncertainty of future conditions. Based on these results and given the relative accessibility of a simulation chain using the LC scenarios associated with each RCP downscaled from Hurtt et al. (2011), LC changes should be incorporated into long-term GWR simulation as much as possible.

The selection of 12 climate scenarios was performed based on the k-means clustering method to capture as much variability as possible in future conditions from the CMIP5 climate simulations based on annual and seasonal ΔT and ΔP. As future climatic conditions simulated using different climate models and different RCPs overlapped, the climate scenarios were selected regardless of the RCP used in their simulation (Dubois et al., 2022). However, this study showed that the intense afforestation simulated for RCP4.5 scenarios produced significant changes in HB_{LC} for smaller changes in climate conditions than were observed for RCP8.5 scenarios (Figure 7). Interestingly, the results obtained for both RCPs mostly overlapped with intense changes in climate conditions. The impact of climate scenario selection on hydrological response to climate change has been addressed by Chen et al. (2016), but was not tested here.

This study showed that the LC change induced changes in GWR also depended on the local geomorphological conditions, meaning that the spatial distribution of the LC changes impacted the changes in GWR. Furthermore, the LC scenarios from Hurtt et al. (2011) simulated a relatively steady LC over time (RCP8.5) in the study area, which corresponds to a "business as usual" scenario, and extreme forest development leading to the near disappearance of agriculture (RCP4.5), whereby most of the agriculture pixels are converted to forest. Although downscaling LC scenarios was straightforward due to these broad changes, it also simulated a RCP4.5 LC scenario that seemed unrealistic for the study area, considering that it is one of the

main agricultural regions in the province of Quebec. The conversion from cropland and pasture land-use classes to secondary lands was represented as changes from agricultural to forested lands following the land use to LC conversion rules from Hurtt et al. (2011), thus leading to afforestation in the RCP4.5 LC scenario. Future work should be dedicated to improving LC downscaling to match observed or anticipated local LC change dynamics and spatial distribution. Regarding the simple downscaling method used for the LC scenarios (from 0.5° x 0.5° to 500 m × 500 m spatial resolution), and since the goal of the study was to compare the ensembles simulated using HB and HB_{LC}, the scenarios of GWR from HB_{LC} should not be used as local estimates of future GWR.

Studies in cold climates with seasonal snowpack have emphasized the role of snow accumulation and melting in GWR (Aygün et al., 2020; Dubois et al., 2022, 2021a; Greenwood & Buttle, 2018; Morgan et al., 2021; Wright & Novakowski, 2020; Young et al., 2019). Winter-related model parameters (snowmelt coefficient, melting temperature, freezing soil) are also known to be very sensitive when simulating cold region hydrology (Dubois et al., 2021a; Mai et al., 2022; Nemri & Kinnard, 2020). More research therefore needs to be dedicated to refining the calibration of winter-related model parameters in LC change contexts.

The simulations in this study were undertaken using a parsimonious superficial water budget that integrated LC classification to estimate runoff through the runoff curve number method and used a temperature-based potential evapotranspiration formula to compute the maximum daily evapotranspiration rate. The runoff curve number method has been proven useful to simulate the impact of land use and LC changes in hydrology (Deshmukh et al., 2013; Isik et al., 2013). It has been used to simulate GWR at the regional scale that captured LC-induced changes coherently with changes in the GWR dynamic observed in other studies in cold climates. Furthermore, the representativeness of LC changes in GWR simulation would most likely be enhanced by integrating a LC based potential evapotranspiration formula that would account for the vegetation dynamics. However, this would also substantially complicate the simulation chain with LC and climate scenarios by requiring more input variables (e.g., leaf area index, relative humidity) depending on both LC and climate scenarios.

The GWR scenarios simulated in this study were based on climate scenarios obtained from the CMIP5 ensemble and the associated LC scenarios provided by Hurtt et al. (2011), and were compared with the results of Dubois et al. (2022). The scenarios of the CMIP6 ensemble are now available, as are the associated land-use harmonization V2 dataset (Hurtt et al., 2020), and the methodology detailed in this paper is expected to be transferrable to these new datasets.

5 | CONCLUSIONS

In cold and humid climates, warming temperatures will result in longer growing seasons, leading to LC changes that could have long-term impacts on GWR. This work has brought new insights about global change impacts on regional-scale GWR. It is the first to produce long-term GWR scenarios based on a combination of LC changes specifically associated with future climate conditions, using two LC scenarios of the land-use harmonization dataset in combination with 12 climate scenarios (RCP4.5 and RCP8.5) to simulate long-term GWR. The simulated GWR scenarios were compared with GWR simulated using the same 12 climate scenarios and a constant LC.

One of the main contributions of this work was to link the increase in GWR simulated with the RCP4.5 scenario (afforestation) to the deficit in snowmelt runoff, thus enhancing snowmelt recharge events and emphasizing the role of the snowmelt parameters in a global change context. GWR was also shown to be more sensitive to changes in temperature and precipitation with intense LC changes, notably because significant GWR changes were produced with a wider range of climatic conditions than when LC was constant. Another outcome of this work was to show that the spatial distribution of LC changes influenced the simulated impact of LC changes on GWR.

This study has confirmed that assessing the impact of global change on GWR is computationally feasible. The results call for a more systematic inclusion of land use and LC changes in long-term simulations, especially as the methodology is expected to be entirely transferrable to the CMIP6 ensemble.

AUTHOR CONTRIBUTIONS

All authors contributed to writing the manuscript and developing the approach. Downscaling of the LC scenarios, simulations, and figure preparation were done by E.D. P.B. hosted E.D. for a research residency to develop the approach. M.L. obtained the research grant and supervised the research. All authors have read and agreed to the published version of the manuscript.

ACKNOWLEDGEMENTS

This research was funded by the Quebec Ministry of Environment and Climate Change (Ministère de l'Environnement et de la Lutte contre les changements climatiques). The authors are grateful to the Ouranos Consortium for providing downscaled climate scenarios and acknowledge the model output data from the World Climate Research Programme's Coupled Modelling Intercomparison Project Phase 5 (CMIP5), as well as the gridded observation data made available by Natural Resources Canada (NRCan). Emmanuel Dubois is also very grateful to the FRQNT, MITACS, and UQAM for the mobility scholarships that provided an opportunity to be a visiting Ph.D. student at the University of Neuchâtel. Open access funding provided by Ecole Polytechnique Federale de Lausanne.

DATA AVAILABILITY STATEMENT

The simulated scenarios presented in this work are available here: https://doi.org/10.5683/SP3/M7SO6Q. The HydroBudget model (Dubois et al., 2021b) is available here: https://doi.org/10.5683/SP3/EUDV3H. The two GWR datasets (Dubois et al., 2021, 2022) presented by Dubois et al. (2021a, 2022) are available here: https://doi.org/10.5683/SP3/TFNPQF and https://doi.org/10.5683/SP3/SWH401.)

ORCID

Emmanuel Dubois https://orcid.org/0000-0003-4896-6368
Marie Larocque https://orcid.org/0000-0001-9906-3535
Philip Brunner https://orcid.org/0000-0001-6304-6274

REFERENCES

Adhikari, R. K., Mohanasundaram, S., & Shrestha, S. (2020). Impacts of land-use changes on the groundwater recharge in the Ho chi Minh city. *Vietnam. Environmental Research*, *185*, 109440. https://doi.org/10.1016/j.envres.2020.109440

Anurag, H., Ng, G. H. C., Tipping, R., & Tokos, K. (2021). Modeling the impact of spatiotemporal vegetation dynamics on groundwater recharge. *Journal of Hydrology*, *601*, 126584. https://doi.org/10.1016/j.jhydrol.2021.126584

Arctic Climate Impact Assessment. (2004). *Impacts of a warming Arctic*. Cambridge University Press.

Assani, A. A., Zeroual, A., Roy, A., & Kinnard, C. (2021). Impacts of agricultural areas on Spatio-temporal variability of daily minimum extreme flows during the transitional seasons (spring and fall) in southern Quebec. *Water*, *13*(24), 3487. https://doi.org/10.3390/w13243487

Atawneh, D. A., Cartwright, N., & Bertone, E. (2021). Climate change and its impact on the projected values of groundwater recharge: A review. *Journal of Hydrology*, *601*, 126602. https://doi.org/10.1016/j.jhydrol.2021.126602

Aygün, O., Kinnard, C., & Campeau, S. (2020). Impacts of climate change on the hydrology of northern midlatitude cold regions. *Progress in Physical Geography: Earth and Environment*, *44*(3), 338–375. https://doi.org/10.1177/0309133319878123

Bergeron, O. (2016). Guide d'utilisation 2016—Grilles climatiques quotidiennes du Programme de surveillance du climat du Québec, version 2 (User guide 2016 – Daily climate grids from the Quebec Climate monitoring program, version 2) (p. 26). ministère du Développement durable, de l'Environnement et de la Lutte contre les changements climatiques, Direction du suivi de l'état de l'environnement [Data set].

Berghuijs, W. R., Woods, R. A., & Hrachowitz, M. (2014). A precipitation shift from snow towards rain leads to a decrease in streamflow. *Nature Climate Change*, *4*(7), 583–586. https://doi.org/10.1038/nclimate2246

Bissonnette, J., Demers, A., & Lavoie, S. (2016). Utilisation du territoire. Méthodologie et description de la couche d'information géographique (Land use. Methodology and overview of the GIS layer) (Version 1.4; p. 24). Gouvernement du Québec, Ministère du Développement durable, de l'Environnement et de la Lutte contre les changements climatiques [Data set].

Brunner, P., Bauer, P., Eugster, M., & Kinzelbach, W. (2004). Using remote sensing to regionalize local precipitation recharge rates obtained from the chloride method. *Journal of Hydrology*, *294*(4), 241–250. https://doi.org/10.1016/j.jhydrol.2004.02.023

Casajus, N., Périé, C., Logan, T., Lambert, M.-C., de Blois, S., & Berteaux, D. (2016). An objective approach to select climate scenarios when projecting species distribution under climate change. *PLoS One*, *11*(3), e0152495. https://doi.org/10.1371/journal.pone.0152495

Chen, J., Brissette, F. P., & Lucas-Picher, P. (2016). Transferability of optimally-selected climate models in the quantification of climate change impacts on hydrology. *Climate Dynamics*, *47*(9), 3359–3372. https://doi.org/10.1007/s00382-016-3030-x

Chini, L. P., Hurtt, G. C., & Frolking, S. (2014). LUH1: Harmonized Global Land Use for Years 1500-2100, V1. [Data set]. https://doi.org/10.3334/ORNLDAAC/1248

Cochand, F., Brunner, P., Hunkeler, D., Rössler, O., & Holzkämper, A. (2021). Cross-sphere modelling to evaluate impacts of climate and land management changes on groundwater resources. *Science of the Total Environment*, *798*, 148759. https://doi.org/10.1016/j.scitotenv.2021.148759

Deshmukh, D. S., Chaube, U. C., Ekube Hailu, A., Aberra Gudeta, D., & Tegene Kassa, M. (2013). Estimation and comparision of curve numbers based on dynamic land use land cover change, observed rainfall-runoff data and land slope. *Journal of Hydrology*, *492*, 89–101. https://doi.org/10.1016/j.jhydrol.2013.04.001

Destouni, G., Jaramillo, F., & Prieto, C. (2013). Hydroclimatic shifts driven by human water use for food and energy production. *Nature Climate Change*, *3*(3), 213–217. https://doi.org/10.1038/nclimate1719

Dubois, E., Larocque, M., & Gagné, S. (2021). 1961–2017 monthly potential groundwater recharge in southern Quebec database [data set]. *Scholars Portal Borealis*. https://doi.org/10.5683/SP3/TFNPQF

Dubois, E., Larocque, M., & Gagné, S. (2022). 12 scenarios of monthly potential groundwater recharge in southern Quebec database – 1951-2100 period [data set]. *Scholars Portal Borealis*. https://doi.org/10.5683/SP3/SWH4O1

Dubois, E., Larocque, M., Gagné, S., & Braun, M. (2022). Climate change impacts on groundwater recharge in cold and humid climates: Controlling processes and thresholds. *Climate*, *10*(1), 6. https://doi.org/10.3390/cli10010006

Dubois, E., Larocque, M., Gagné, S., & Meyzonnat, G. (2021a). Simulation of long-term spatiotemporal variations in regional-scale groundwater recharge: Contributions of a water budget approach in cold and humid climates. *Hydrology and Earth System Sciences*, *25*(12), 6567–6589. https://doi.org/10.5194/hess-25-6567-2021

Dubois, E., Larocque, M., Gagné, S., & Meyzonnat, G. (2021b). HydroBudget – Groundwater recharge model in R [code]. *Scholars Portal Borealis*. https://doi.org/10.5683/SP3/EUDV3H

Foster, S., & Ait-Kadi, M. (2012). Integrated water resources management (IWRM): How does groundwater fit in? *Hydrogeology Journal*, *20*(3), 415–418. https://doi.org/10.1007/s10040-012-0831-9

Gagné, G., Beaudin, I., Leblanc, M., Drouin, A., Veilleux, G., Sylvain, J.-D., & Michaud, A. (2013). Classement des séries de sols minéraux du Québec selon les groupes hydrologiques (Classification of Quebec mineral soil types by hydrologic groups, final report) (p. 81) [method]. https://www.irda.qc.ca/assets/documents/Publications/documents/gagne-et-al-2013_rapport_classement_sols_mineraux_groupes_hydro.pdf

Ghimire, U., Shrestha, S., Neupane, S., Mohanasundaram, S., & Lorphensri, O. (2021). Climate and land-use change impacts on spatiotemporal variations in groundwater recharge: A case study of the Bangkok area. *Thailand. Science of the Total Environment*, *792*, 148370. https://doi.org/10.1016/j.scitotenv.2021.148370

Goodbrand, A., Anderson, A., Devito, K., & Silins, U. (2022). Untangling harvest-streamflow responses in foothills conifer forests: Nexus of teleconnections, summer-dominated precipitation, and storage. *Hydrological Processes*, *36*(2), e14479. https://doi.org/10.1002/hyp.14479

Greenwood, W. J., & Buttle, J. M. (2018). Land cover controls on depression-focused recharge on the oak ridges moraine, southern Ontario, Canada. *Hydrological Processes*, *32*(12), 1909–1926. https://doi.org/10.1002/hyp.13130

Guerrero-Morales, J., Fonseca, C. R., Goméz-Albores, M. A., Sampedro-Rosas, M. L., & Silva-Gómez, S. E. (2020). Proportional variation of potential groundwater recharge as a result of climate change and land-use: A study case in Mexico. *Land*, *9*(10). https://doi.org/10.3390/land9100364

Healey, N. C., & Rover, J. A. (2022). Analyzing the effects of land cover change on the water balance for case study watersheds in different forested ecosystems in the USA. *Land*, *11*(2), 316. https://doi.org/10.3390/land11020316

Hopkinson, R. F., McKenney, D. W., Milewska, E. J., Hutchinson, M. F., Papadopol, P., & Vincent, L. A. (2011). Impact of aligning climatological day on gridding daily maximum–minimum temperature and precipitation over Canada. *Journal of Applied Meteorology and Climatology*, *50*(8), 1654–1665. https://doi.org/10.1175/2011JAMC2684.1

Hurtt, G. C., Chini, L., Sahajpal, R., Frolking, S., Bodirsky, B. L., Calvin, K., Doelman, J. C., Fisk, J., Fujimori, S., Klein Goldewijk, K., Hasegawa, T., Havlik, P., Heinimann, A., Humpenöder, F., Jungclaus, J., Kaplan, J. O., Kennedy, J., Krisztin, T., Lawrence, D., … Zhang, X. (2020). Harmonization of global land use change and management for the period 850–

2100 (LUH2) for CMIP6. *Geoscientific Model Development*, *13*(11), 5425–5464. https://doi.org/10.5194/gmd-13-5425-2020

Hurtt, G. C., Chini, L. P., Frolking, S., Betts, R. A., Feddema, J., Fischer, G., Fisk, J. P., Hibbard, K., Houghton, R. A., Janetos, A., Jones, C. D., Kindermann, G., Kinoshita, T., Klein Goldewijk, K., Riahi, K., Shevliakova, E., Smith, S., Stehfest, E., Thomson, A., … Wang, Y. P. (2011). Harmonization of land-use scenarios for the period 1500–2100: 600 years of global gridded annual land-use transitions, wood harvest, and resulting secondary lands. *Climatic Change*, *109*(1), 117–161. https://doi.org/10.1007/s10584-011-0153-2

Hutchinson, M. F., McKenney, D. W., Lawrence, K., Pedlar, J. H., Hopkinson, R. F., Milewska, E., & Papadopol, P. (2009). Development and testing of Canada-wide interpolated spatial models of daily minimum–maximum temperature and precipitation for 1961–2003. *Journal of Applied Meteorology and Climatology*, *48*(4), 725–741. https://doi.org/10.1175/2008JAMC1979.1

Hwang, T., Martin, K. L., Vose, J. M., Wear, D., Miles, B., Kim, Y., & Band, L. E. (2018). Nonstationary hydrologic behavior in forested watersheds is mediated by climate-induced changes in growing season length and subsequent vegetation growth. *Water Resources Research*, *54*(8), 5359–5375. https://doi.org/10.1029/2017WR022279

Institut de recherche et développement en agroenvironnement [IRDA]. (2008). Feuillets pédologiques numériques (Numeric pedology maps) (Données du Ministère de l'Agriculture, des Pêcheries et de l'Alimentation du Québec (MAPAQ) et de l'Institut de recherche et développement en agroenvironnement (IRDA)) [Map].

Isik, S., Kalin, L., Schoonover, J. E., Srivastava, P., & Graeme Lockaby, B. (2013). Modeling effects of changing land use/cover on daily streamflow: An artificial neural network and curve number based hybrid approach. *Journal of Hydrology*, *485*, 103–112. https://doi.org/10.1016/j.jhydrol.2012.08.032

Jaramillo, F., Prieto, C., Lyon, S. W., & Destouni, G. (2013). Multimethod assessment of evapotranspiration shifts due to non-irrigated agricultural development in Sweden. *Journal of Hydrology*, *484*, 55–62. https://doi.org/10.1016/j.jhydrol.2013.01.010

King, M., Altdorff, D., Li, P., Galagedara, L., Holden, J., & Unc, A. (2018). Northward shift of the agricultural climate zone under 21st-century global climate change. *Scientific Reports*, *8*(1), 7904. https://doi.org/10.1038/s41598-018-26321-8

Klein Goldewijk, K., Beusen, A., & Janssen, P. (2010). Long-term dynamic modeling of global population and built-up area in a spatially explicit way: HYDE 3.1. *The Holocene*, *20*(4), 565–573. https://doi.org/10.1177/0959683609356587

Kløve, B., Ala-Aho, P., Bertrand, G., Gurdak, J. J., Kupfersberger, H., Kværner, J., Muotka, T., Mykrä, H., Preda, E., Rossi, P., Uvo, C. B., Velasco, E., & Pulido-Velazquez, M. (2014). Climate change impacts on groundwater and dependent ecosystems. *Journal of Hydrology*, *518*, 250–266. https://doi.org/10.1016/j.jhydrol.2013.06.037

Larocque, M., Levison, J., Martin, A., & Chaumont, D. (2019). A review of simulated climate change impacts on groundwater resources in eastern Canada. *Canadian Water Resources Journal [Revue Canadienne des Ressources Hydriques]*, *44*(1), 22–41. https://doi.org/10.1080/07011784.2018.1503066

Mai, J., Craig, J. R., Tolson, B. A., & Arsenault, R. (2022). The sensitivity of simulated streamflow to individual hydrologic processes across North America. *Nature Communications*, *13*(1), 455. https://doi.org/10.1038/s41467-022-28010-7

Mohan, C., Western, A. W., Wei, Y., & Saft, M. (2018). Predicting groundwater recharge for varying land cover and climate conditions – A global meta-study. *Hydrology and Earth System Sciences*, *22*(5), 2689–2703. https://doi.org/10.5194/hess-22-2689-2018

Monfet, J. (1979). Evaluation du coefficient de ruissellement à l'aide de la méthode SCS modifiée (Evaluation of the runoff coefficient computation with the modified SCS method) [method]. Bibliothèque nationale du Québec.

Morgan, L. R., Hayashi, M., & Cey, E. E. (2021). Land-use comparison of depression-focussed groundwater recharge in the Canadian prairies. *Hydrological Processes*, *35*(9), e14379. https://doi.org/10.1002/hyp.14379

Mpelasoka, F. S., & Chiew, F. H. S. (2009). Influence of rainfall scenario construction Methods on runoff projections. *Journal of Hydrometeorology*, *10*(5), 1168–1183. https://doi.org/10.1175/2009JHM1045.1

Nemri, S., & Kinnard, C. (2020). Comparing calibration strategies of a conceptual snow hydrology model and their impact on model performance and parameter identifiability. *Journal of Hydrology*, *582*, 124474. https://doi.org/10.1016/j.jhydrol.2019.124474

NRCan. (2021). ISO 19131 – Land Use 1990, 2000 & 2010 Data Product Specification. http://www.agr.gc.ca/atlas/supportdocument_documentdesupport/aafcLand_Use/en/ISO_19131_Land_Use_1990__2000_2010_Data_Product_Specifications.pdf [Web page, last access 2021-09-30].

Nygren, M., Giese, M., Kløve, B., Haaf, E., Rossi, P. M., & Barthel, R. (2020). Changes in seasonality of groundwater level fluctuations in a temperate-cold climate transition zone. *Journal of Hydrology X*, *8*, 100062. https://doi.org/10.1016/j.hydroa.2020.100062

Oudin, L., Hervieu, F., Michel, C., Perrin, C., Andréassian, V., Anctil, F., & Loumagne, C. (2005). Which potential evapotranspiration input for a lumped rainfall–runoff model? Part 2—Towards a simple and efficient potential evapotranspiration model for rainfall–runoff modelling. *Journal of Hydrology*, *303*(1), 290–306. https://doi.org/10.1016/j.jhydrol.2004.08.026

Pi, K., Bieroza, M., Brouchkov, A., Chen, W., Dufour, L. J. P., Gongalsky, K. B., Herrmann, A. M., Krab, E. J., Landesman, C., Laverman, A. M., Mazei, N., Mazei, Y., Öquist, M. G., Peichl, M., Pozdniakov, S., Rezanezhad, F., Roose-Amsaleg, C., Shatilovich, A., Shi, A., … Van Cappellen, P. (2021). The cold region critical zone in transition: Responses to climate warming and land use change. *Annual Review of Environment and Resources*, *46*(1), 111–134. https://doi.org/10.1146/annurev-environ-012220-125703

Quilbé, R., Rousseau, A. N., Moquet, J.-S., Savary, S., Ricard, S., & Garbouj, M. S. (2008). Hydrological responses of a watershed to historical land use evolution and future land use scenarios under climate change conditions. *Hydrology and Earth System Sciences*, *12*(1), 101–110. https://doi.org/10.5194/hess-12-101-2008

Riahi, K., Rao, S., Krey, V., Cho, C., Chirkov, V., Fischer, G., Kindermann, G., Nakicenovic, N., & Rafaj, P. (2011). RCP 8.5—A scenario of comparatively high greenhouse gas emissions. *Climatic Change*, *109*(1), 33–57. https://doi.org/10.1007/s10584-011-0149-y

Rivera, A. (2014). *Canada's groundwater resources*. Fitzhenry & Whiteside.

Shuler, C., Brewington, L., & El-Kadi, A. I. (2021). A participatory approach to assessing groundwater recharge under future climate and land-cover scenarios, Tutuila, American Samoa. *Journal of Hydrology: Regional Studies*, *34*, 100785. https://doi.org/10.1016/j.ejrh.2021.100785

Smerdon, B. D. (2017). A synopsis of climate change effects on groundwater recharge. *Journal of Hydrology*, *555*, 125–128. https://doi.org/10.1016/j.jhydrol.2017.09.047

Taylor, K. E., Stouffer, R. J., & Meehl, G. A. (2012). An overview of CMIP5 and the experiment design. *Bulletin of the American Meteorological Society*, *93*(4), 485–498. https://doi.org/10.1175/BAMS-D-11-00094.1

Taylor, R. G., Scanlon, B., Döll, P., Rodell, M., van Beek, R., Wada, Y., Longuevergne, L., Leblanc, M., Famiglietti, J. S., Edmunds, M., Konikow, L., Green, T. R., Chen, J., Taniguchi, M., Bierkens, M. F. P., MacDonald, A., Fan, Y., Maxwell, R. M., Yechieli, Y., … Treidel, H. (2013). Ground water and climate change. *Nature Climate Change*, *3*(4), 322–329. https://doi.org/10.1038/nclimate1744

Thomson, A. M., Calvin, K. V., Smith, S. J., Kyle, G. P., Volke, A., Patel, P., Delgado-Arias, S., Bond-Lamberty, B., Wise, M. A., Clarke, L. E., & Edmonds, J. A. (2011). RCP4.5: A pathway for stabilization of radiative forcing by 2100. *Climatic Change*, *109*(1), 77–94. https://doi.org/10.1007/s10584-011-0151-4

USDA-NRCS. (2004). *Chapter 9 hydrologic soil-cover complexes*. United State Department of Agriculture-Natural Ressources Conservation Service [Method]. https://www.nrcs.usda.gov/Internet/FSE_DOCUMENTS/stelprdb1043088.pdf

USDA-NRCS. (2007). *Chapter 7 hydrologic soil groups* (2009th ed.). United State Department of Agriculture-Natural Ressources Conservation Service [method]. https://directives.sc.egov.usda.gov/OpenNonWebContent.aspx?content=22526.wba

van Vuuren, D. P., Edmonds, J., Kainuma, M., Riahi, K., Thomson, A., Hibbard, K., Hurtt, G. C., Kram, T., Krey, V., Lamarque, J.-F., Masui, T., Meinshausen, M., Nakicenovic, N., Smith, S. J., & Rose, S. K. (2011). The representative concentration pathways: An overview. *Climatic Change*, *109*(1), 5–31. https://doi.org/10.1007/s10584-011-0148-z

Verburg, P. H., Neumann, K., & Nol, L. (2011). Challenges in using land use and land cover data for global change studies. *Global Change Biology*, *17*(2), 974–989. https://doi.org/10.1111/j.1365-2486.2010.02307.x

Wada, Y., van Beek, L. P. H., van Kempen, C. M., Reckman, J. W. T. M., Vasak, S., & Bierkens, M. F. P. (2010). Global depletion of groundwater resources. *Geophysical Research Letters*, *37*(20), 5. https://doi.org/10.1029/2010GL044571

Wright, S. N., & Novakowski, K. S. (2020). Impacts of warming winters on recharge in a seasonally frozen bedrock aquifer. *Journal of Hydrology*, *590*, 125352. https://doi.org/10.1016/j.jhydrol.2020.125352

Young, D., Zégre, N., Edwards, P., & Fernandez, R. (2019). Assessing streamflow sensitivity of forested headwater catchments to disturbance and climate change in the central Appalachian Mountains region, USA. *Science of the Total Environment*, *694*, 133382. https://doi.org/10.1016/j.scitotenv.2019.07.188

Zhang, Z., Li, M., Si, B., & Feng, H. (2018). Deep rooted apple trees decrease groundwater recharge in the highland region of the loess plateau, China. *Science of the Total Environment*, *622–623*, 584–593. https://doi.org/10.1016/j.scitotenv.2017.11.230

Zhang, Z., Wang, W., Gong, C., Zhao, M., Franssen, H.-J. H., & Brunner, P. (2021). Salix psammophila afforestations can cause a decline of the water table, prevent groundwater recharge and reduce effective infiltration. *Science of the Total Environment*, *780*, 146336. https://doi.org/10.1016/j.scitotenv.2021.146336

Zomlot, Z., Verbeiren, B., Huysmans, M., & Batelaan, O. (2017). Trajectory analysis of land use and land cover maps to improve spatial–temporal patterns, and impact assessment on groundwater recharge. *Journal of Hydrology*, *554*, 558–569. https://doi.org/10.1016/j.jhydrol.2017.09.032

SUPPORTING INFORMATION

Additional supporting information can be found online in the Supporting Information section at the end of this article.

How to cite this article: Dubois, E., Larocque, M., & Brunner, P. (2023). Impact of land cover changes on Long-Term Regional-Scale groundwater recharge simulation in cold and humid climates. *Hydrological Processes*, *37*(2), e14810. https://doi.org/10.1002/hyp.14810